JOURNAL OF THERMOPHYSICS AND HEAT TRANSFER
Vol. 11, No. 3, July–September 1997

Laminar Pulsed Forced and Mixed Convection in a Vertical Isothermal Tube

T. A. Myrum,* S. Acharya,† and S. Inamdar‡
Louisiana State University, Baton Rouge, Louisiana 70803

Numerical fluid flow and heat transfer results were obtained for a pulsed laminar flow through a vertical, isothermal-walled tube for $Gr/Re = 0$ (no buoyancy) and 30 (buoyancy) at a cyclic-averaged Reynolds number of 5×10^2. The pulsations resulted in cyclic-averaged Nusselt numbers Nu_{av} that were greater than the steady, fully developed laminar Nusselt number, with Nu_{av} increasing with increasing frequency. The Nusselt number also increased with increasing amplitude a for $Gr/Re = 0$, but it remained virtually constant beyond $a = 0.1$ for $Gr/Re = 30$. Although the Nu_{av} values at $Gr/Re = 30$ were greater than at $Gr/Re = 0$, they were offset by relatively large values of the cyclic-averaged dimensionless wall shear stress τ_{av}. For $Gr/Re = 30$, Nu_{av}/τ_{av} was either the same or less than that for steady, fully developed laminar flow. Conversely, Nu_{av}/τ_{av} increased by as much as 39% for $Gr/Re = 0$.

Nomenclature

a = pulsation amplitude
c_v = specific heat at constant volume
f = frequency
Gr = Grashof number, $g\beta(T_0 - T_w)r_0^3/\nu^2$
h_i = instantaneous heat transfer coefficient, $[k(\partial T/\partial r)_{r=r_0}]/(T_w - T_b)$
k = thermal conductivity
Nu_{av} = cyclic-averaged Nusselt number, $1/\hat{\tau}_p(\int_0^{\hat{\tau}_p} Nu_i \, d\hat{\tau})$
Nu_i = instantaneous Nusselt number, $2h_i r_0/k$
P = dimensionless pressure, $(p + \rho g z)/(\rho_0 u_0^2)$
Pe = modified Peclet number, $Re(c_v\mu/k)$, 252.5
p = pressure
R = dimensionless radial coordinate, r/r_0
Re = cyclic-averaged Reynolds number, $2r_0u_0/\nu$, 5×10^2
r = radial coordinate
r_0 = radius of tube
T = temperature
T_b = bulk temperature
T_w = tube-wall temperature
T_0 = fluid entrance temperature
t = time
t_p = forcing period, $1/f$
U = dimensionless axial velocity, u/u_0
u = axial velocity
u_0 = fluid entrance velocity, cyclic-averaged velocity
V = instantaneous dimensionless radial velocity, v/u_0
v = radial velocity
Z = dimensionless axial coordinate, z/r_0
z = axial coordinate
θ = dimensionless temperature, $(T - T_0)/(T_w - T_0)$
μ = dynamic viscosity
ν = kinematic viscosity, μ/ρ
ρ = mass density
$\hat{\tau}$ = dimensionless time, $t/(r_0/u_0)$
τ_{av} = cyclic-averaged dimensionless wall shear stress, $1/\hat{\tau}_p(\int_0^{\hat{\tau}_p} \tau_{wi} \, d\hat{\tau})$
$\hat{\tau}_p$ = dimensionless period, $t_p/(r_0/u_0)$
τ_{wi} = instantaneous dimensionless wall shear stress, $[-\mu(\partial u/\partial r)_{r=r_0}]/\rho_0 u_0^2$

Received May 13, 1996; revision received March 14, 1997; accepted for publication March 14, 1997.

*Associate Professor, Mechanical Engineering Department.
†L. R. Daniel Professor, Mechanical Engineering Department.
‡Graduate Student, Mechanical Engineering Department.

Introduction

IN response to the heat transfer problems associated with the operation of the internal combustion engine, Martinelli et al.[1] were the first to study the heat transfer in pulsed flows. Basically, they showed, as a first approximation, that steady flow data may be used to predict the heat transfer performance in pulsating flows.

Subsequently, in a series of studies, the effect of resonant acoustic excitations on the heat transfer to airflows through tubes was investigated. Jackson et al.[2] found excitations above 118 db to suppress natural convection; Lemlich and Hwu[3] found that acoustic excitations produced increases of up to 51 and 27% in the laminar and turbulent regimes, respectively. The improvement peaked sharply at resonance and increased with the resonant frequency and amplitude. Purdy et al.[4] and Jackson and Purdy[5] also found enhancements in heat transfer with flow pulsations.

Grassmann and Tuma[6] pulsed a flow using a bellows pump. The pulsations produced mean Sherwood numbers that were 2.5 times those for steady flows. A pulsating turbulent pipe flow was studied using a laser-Doppler velocimeter by Kirmse[7]; Ramaprian and Tu[8] sinusoidally pulsed an oil flow between a minimum Reynolds number of 1.278×10^3 and a maximum Reynolds number of 2.872×10^3.

Creff et al.[9] developed a numerical model to analyze the simultaneous development of the hydrodynamic and thermal regimes of a sinusoidally pulsed laminar flow through a tube. It was concluded from temperature and velocity profiles that far from the tube inlet, the pulsations would not result in increased heat transfer.

Liao et al.[10] investigated the heat transfer in a pulsating turbulent flow. It was found for the Reynolds number range of 3.4×10^3 to 2.7×10^4 that the heat transfer coefficients with pulsation were reduced and that the extent of the reduction depended mainly on the amplitude. They classified their data and the data from other investigations into three regions: 1) quasi-steady-state, 2) frequency independent, and 3) frequency dependent. Increases in the heat transfer were concluded to be possible only in the frequency-dependent region.

The numerical simulations of Siegal[11] demonstrated for uniformly heated, laminar flows with low Peclet numbers that flow pulsations lead to a reduction in the duct heat transfer coefficient. This was attributed to the fact that the flow pul-

sations provide for the axial transport of energy in the upstream direction, which in turn acts to preheat the flow.

Dec and Keller[12] experimentally studied the heat transfer that arises in the tail pipe of a pulse combustor. They pointed out that the high heat transfer rate in the tail pipe caused by the pulsations is one of the advantages of pulse combustors. It was found that the Nusselt number increased with both pulsation amplitude and frequency, with the maximum increase being 2.5 times that for steady flow at the same mean Reynolds number.

All of the studies cited previously deal with pulsed forced convection situations. The purpose of the present investigation is to examine the effect of buoyancy on the heat transfer and flow behavior in a pulsed laminar airflow through a vertical, isothermal-walled tube. To this end, the Boussinesq-approximated parabolized equations are solved numerically for sinusoidal-like velocity pulsations superposed on a steady flow. Flow pulsations were accomplished by varying the flow at the inlet to the tube according to the absolute value of the sine function. Only aided buoyancy, where the pulsating forced flow and the buoyancy-induced flow are in the same direction, is considered in this paper.

Instantaneous and cyclic-averaged Nusselt number and dimensionless wall shear stress results, as well as instantaneous radial velocity and temperature profiles, were obtained at a cyclic-averaged Reynolds number of 5×10^2 for amplitudes ranging from 10 to 80% of the uniform inlet velocity u_0 at a fixed frequency of 5 Hz and for frequencies ranging from 2 to 60 Hz at a fixed amplitude of $0.10u_0$. To assess the role of buoyancy, results are obtained for flows with ($Gr/Re = 30$) and without ($Gr/Re = 0$) buoyancy. All of the results are presented at the axial location ($Z/Pe = 1.07$), where steady, laminar flow is fully developed and the bulk flow temperature is very close (within 1%) to the wall temperature.[13] Therefore, the steady flow results are independent of Gr/Re.

Calculations

The problem was simplified by using the Boussinesq-approximated parabolized equations for an incompressible flow with negligible viscous dissipation. In dimensionless form, the governing equations and their boundary conditions, written for the flow situation depicted in Fig. 1, are

$$\frac{\partial U}{\partial Z} + \frac{1}{R}\frac{\partial (RV)}{\partial R} = 0 \tag{1}$$

$$\frac{\partial U}{\partial \hat{\tau}} + U\frac{\partial U}{\partial Z} + V\frac{\partial U}{\partial R} = -\frac{dP}{dZ} + \frac{2}{Re}\left[\frac{1}{R}\frac{\partial}{\partial R}\left(R\frac{\partial U}{\partial R}\right)\right] + \frac{4Gr\theta}{Re^2} \tag{2}$$

$$\frac{\partial \theta}{\partial \hat{\tau}} + U\frac{\partial \theta}{\partial z} + V\frac{\partial \theta}{\partial R} = \frac{2}{Pe}\left[\frac{1}{R}\frac{\partial}{\partial R}\left(R\frac{\partial \theta}{\partial R}\right)\right] \tag{3}$$

$$U(\hat{\tau}, R, 0) = U_i(\hat{\tau}), \qquad \theta(\hat{\tau}, R, 0) = 0 \tag{4}$$

$$\left(\frac{\partial U}{\partial R}\right)_{\tau,0,Z} = 0, \qquad \left(\frac{\partial \theta}{\partial R}\right)_{\tau,0,Z} = 0 \tag{5}$$

$$U(\hat{\tau}, 1, Z) = 0, \qquad \theta(\tau, 1, Z) = 1 \tag{6}$$

where Eqs. (4), (5), and (6) are the boundary conditions at the tube inlet, centerline, and wall, respectively, the dimensionless quantities are defined in the Nomenclature, and

$$U_i(\hat{\tau}) = (1 - a) + (\pi/2)a\left|\sin[\pi f(r_0/u_0)\hat{\tau}]\right| \tag{7}$$

When averaged over the forcing cycle (0 to π), the dimensional form of Eq. (7) gives the time-averaged velocity u_0 of the unforced case. The Reynolds number based on u_0 has been selected to be 5×10^2 to match the unforced case of Zeldin and Schmidt.[13] It should be mentioned that Eq. (3) is the constant-volume-specific-heat form of the energy equation used by Zeldin and Schmidt.[13] Note, Eq. (7) only takes the positive portion of the sine function, and in this respect, the pulsations are not truly sinusoidal and the period of each pulsation is π instead of 2π. The velocities are therefore always positive in the streamwise direction with a constant part ($=1 - a$) and a positive time-varying part. In view of this, and the fact that the Peclet number ($RePr$) is quite high ($=252.5$), parabolic flow assumptions are justified. Further, at the low Reynolds number of interest to this study, compressibility effects are assumed to be small.

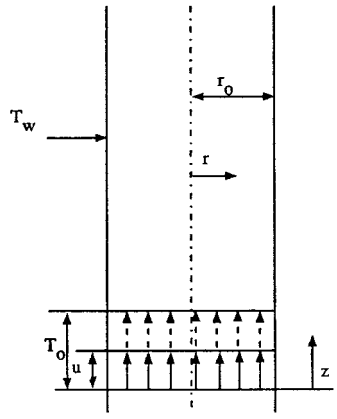

Fig. 1 Flow configuration.

In Eqs. (2) and (3), the V velocities are computed using the mass conservation equations [Eq. (1)]. The pressure gradient appearing in Eq. (2) is obtained by requiring the overall mass to be conserved at every forward step. This approach has been widely used for two-dimensional developing parabolic (or boundary-layer) flows.

Numerical solutions of the nondimensional governing equations were obtained using the Patankar–Spalding finite difference procedure.[14] This scheme is a control-volume-based marching technique, which begins at the tube entrance and proceeds up to the desired axial location. A coordinate transformation is used that maps the boundary-layer region into a uniform computational domain. Thus, as the flow develops, grid points are always confined to the boundary-layer region and are not wasted in the potential core portion of the flow. At each downstream step, the parabolic governing equations are expressed in an integral form, with profile approximations made in both coordinate directions. A tridiagonal system of equations is obtained at each downstream location and is solved using the Tri-Diagonal Matrix Algorithm (TDMA), details of which are given in Patankar and Spalding.[14]

Since the solution at each time step required a complete solution at the preceding time step, a time-marching solution process was employed. The process was initiated at $\hat{\tau} = 0$ with an initial velocity and temperature field ($U = 1$ and $\theta = 0$, respectively). Then, using the tube inlet conditions specified in Eq. (4) and marching downstream from the tube inlet to the desired axial location ($Z/Pe = 1.07$), a set of solutions was obtained over the desired length at the first time step. For the next time step, the inlet flow velocity $U_i(\hat{\tau})$ was changed using Eq. (7), and the marching procedure was repeated, yielding a complete set of solutions at the second time step. This process was continued until a complete set of solutions was obtained at every time step in the excitation cycle.

Solutions for the subsequent cycles were obtained in a similar manner, with the solution at the last time step of the previous cycle used as the initial solution for the current cycle. The solution procedure was continued until a converged solution was obtained. A solution was said to be converged when the solutions for two consecutive cycles failed to produce ad-

ditional changes (to five significant figures) in temperatures and velocities at $Z/Pe = 1.07$ at four representative time steps in the cycle.

Results and Discussion

The heat transfer results are presented at $Z/Pe = 1.07$ in terms of the instantaneous Nusselt number, which is defined as

$$Nu_i = 2r_0 h_i/k, \quad h_i = k\left(\frac{\partial T}{\partial r}\right)_{r=r_0} \Big/ T_w - T_b$$
$$T_b = \int_0^{r_0} rTu \, dr \Big/ \int_0^{r_0} ru \, du \tag{8}$$

and the cyclic-averaged Nusselt number

$$Nu_{av} = \frac{1}{\hat{\tau}_p}\int_0^{\hat{\tau}_p} Nu_i \, d\hat{\tau} \tag{9}$$

Also, of interest at $Z/Pe = 1.07$, was the instantaneous dimensionless wall shear stress

$$\tau_{wi} = -\mu\left(\frac{\partial u}{\partial r}\right)_{r=r_0} \Big/ \rho u_0^2 \tag{10}$$

and the associated cyclic-averaged dimensionless wall shear stress

$$\tau_{av} = \frac{1}{\hat{\tau}_p}\int_0^{\hat{\tau}_p} \tau_{wi} \, d\hat{\tau} \tag{11}$$

Results are presented for $Gr/Re = 0$ and $Gr/Re = 30$. The choice of Gr/Re as the buoyancy parameter needs further explanation. When the equations are expressed in primitive variables and nondimensionalized as done in this paper, Gr/Re^2 emerges as the nondimensional parameter. When the equations are cast in a stream function and vorticity formulation, as Zeldin and Schmidt[13] did, Gr/Re appears as the parameter. There is some disagreement in the literature between the choice of Gr/Re and Gr/Re^2. Since, in this paper, results are compared with those of Zeldin and Schmidt's,[13] their choice of Gr/Re is retained here as the appropriate parameter.

Grid and Time-Step Independence and Solution Validation

Figure 2 demonstrates that the instantaneous Nusselt number computed on a 100 (cross stream) by 200 (axial) grid with a dimensionless time step of $\Delta\hat{\tau} = 1.0$ agrees quite well with that computed on a 150 by 280 grid with $\Delta\hat{\tau} = 0.7$. Therefore, the solutions presented in this study were obtained on a 100 by 200 grid with $\Delta\hat{\tau} = 1.0$.

To test the validity of the simplified governing equations and the solution process, the steady-state form of Eqs. (2) and (3) were solved for the steady version of the boundary conditions of Eqs. (4–6) with $U(R, 0) = 1$. The steady solution also provided an unexcited baseline, to which the excited cases were compared.

The steady-state velocity profiles are compared to the profiles of Zeldin and Schmidt[13] at three different axial locations in Fig. 3. Zeldin and Schmidt's[13] profiles were obtained by solving the elliptic form of the governing equations. At $Z/Pe = 0.011$ and 0.060, the results are for $Re = 5 \times 10^2$, $Pe = 252.5$, and $Gr/Re = 30$; whereas at $Z/Pe = 1.07$, $Re = 3.798 \times 10^3$, $Pe = 191.8$, and $Gr/Re = 33.25$. The velocity measurements of Zeldin and Schmidt[13] are also included for $Z/Pe = 1.07$. It is seen that there is excellent agreement between the results of this study and those of Ref. 13. In addition, the steady-state local Nusselt numbers calculated in this study are virtually identical to those calculated by Zeldin and Schmidt[13] at all three axial locations.

Amplitude Effect

Figure 4 examines the effect of the pulsing amplitude a on the cyclic-averaged Nusselt number and cyclic-averaged dimensionless wall shear stress. Converged solutions could only be obtained for amplitudes up to 0.8 and 0.4 for $Gr/Re = 0$ and 30, respectively.

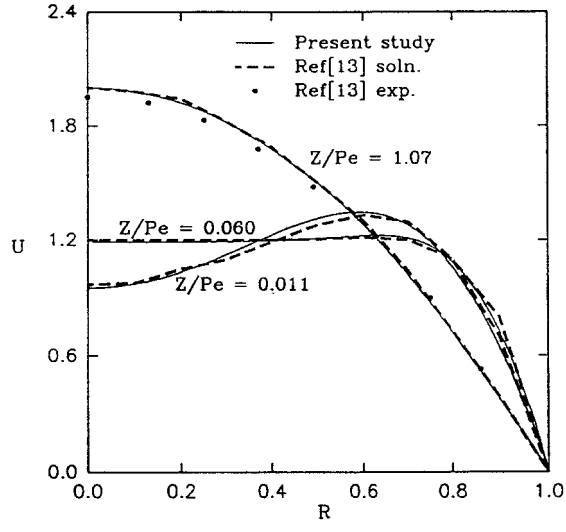

Fig. 3 Comparison between the steady-state velocity profiles of the present study and those of Ref. 13.

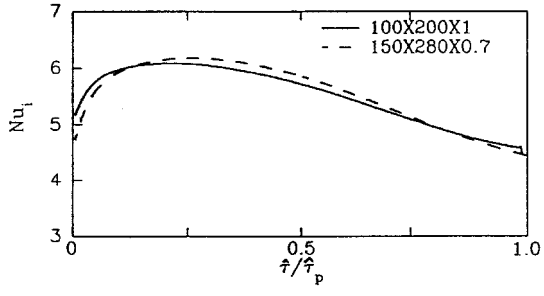

Fig. 2 Comparison of instantaneous Nusselt numbers for two grid sizes.

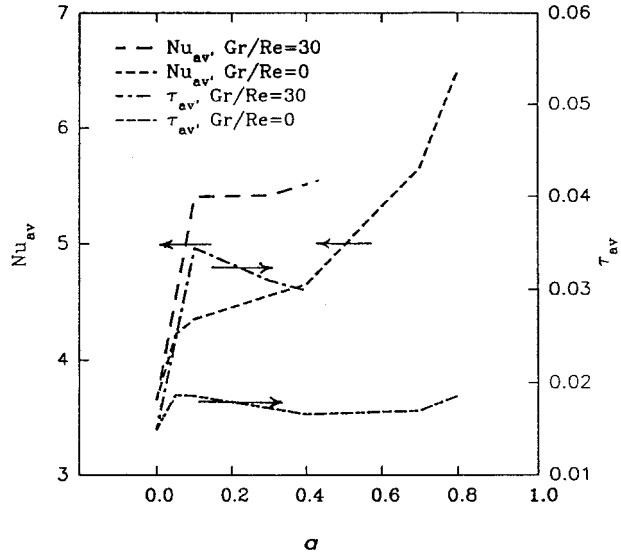

Fig. 4 Effect of amplitude on the cyclic-averaged Nusselt number and dimensionless wall shear stress at 5 Hz.

Figure 4 shows that for both Gr/Re values, the initiation of the excitations results in increased average Nusselt numbers, with the initial increase being more pronounced for Gr/Re = 30. Over the range of amplitudes considered, the average Nusselt number remains nearly constant beyond a = 0.1 for Gr/Re = 30; whereas for Gr/Re = 0, the average Nusselt number increases with increasing amplitude. The average dimensionless wall shear stress for Gr/Re = 0 is seen to remain nearly constant over the amplitude range; whereas for Gr/Re = 30, after a substantial initial increase, the average wall shear decays over the amplitude range.

To explain the previously mentioned behavior, it should be noted that in all cases the cycle-averaged Reynolds number is the same. Therefore, when a is larger, the cyclic variations in velocity (or Re) will be greater, with some portions of the cycle associated with lower instantaneous velocities, and therefore lower instantaneous wall shear and heat transfer (see Fig. 5), and other portions associated with greater velocity and larger wall shear and heat transfer rates. The cycle-averaged value shown in Fig. 4 represents the cumulative effect of the instantaneous variations in a cycle. For Gr/Re = 30, until a = 0.1, the cumulative effect of the increases in wall shear and heat transfer are larger, and an increase in the cycle-averaged value of these quantities are observed. Beyond this value of a, for the heat transfer the increases in one portion of the cycle are balanced by decreases in the other portions of the cycle, and the Nusselt number is relatively insensitive to a. However, for the wall shear, there is a decrease beyond a = 0.1, indicating that the instantaneous reductions in the wall shear are more significant than the instantaneous enhancements in the shear during one cycle.

It is also important to examine the effect of the excitations on Nu_{av}/τ_{av}. At a = 0.4, the excitations result in a 13% increase in Nu_{av}/τ_{av} for Gr/Re = 0 and a 25% decrease in Nu_{av}/τ_{av} for Gr/Re = 30 compared to that for steady, fully developed, laminar flow (a = 0). The maximum increase of 39% occurs for Gr/Re = 0 at a = 0.8.

Cyclic variations of the instantaneous Reynolds number Re_i, Nusselt number Nu_i, and dimensionless wall shear stress τ_{wi} are displayed in Fig. 5 at different amplitudes for Gr/Re = 30 and f = 5 Hz. As expected, the instantaneous Nusselt number and wall shear stress exhibit the same general trends, with the cyclic variation in both increasing with increases in the cyclic variation of Re_i, as dictated by increases in the forcing amplitude. Figure 5 also shows that both the Nu_i and τ_{wi} distributions are distorted from the sinusoidal Re_i distribution, with the peak Nu_i and τ_{wi} values occurring before the peak Re_i value.

It is seen that Nu_i attains its peak value more quickly than τ_{wi} and decays more slowly. The peak Nu_i time at a = 0.1 is observed to be closer to the peak Re_i time than at a = 0.4. Conversely, the peak τ_{wi} time at a = 0.4 is closer to the peak Re_i time than at a = 0.1. Moreover, the difference between the peak Nu_i and τ_{wi} times increases considerably between a = 0.1 and 0.3, but it remains virtually the same between a = 0.3 and 0.4.

With the intent of rationalizing why the peak Re_i, Nu_i, and τ_{wi} values occur at different times, Fig. 6 presents the instantaneous radial velocity and temperature profiles for a = 0.4 and f = 5 Hz at the maximum Nu_i, τ_{wi}, and Re_i instants: $\hat{\tau}/\hat{\tau}_p$ = 0.17, 0.31, and 0.50, respectively. The velocity profiles show that as Re_i increases between $\hat{\tau}/\hat{\tau}_p$ = 0.17 and 0.31, the velocity increases, causing a decrease in the momentum boundary-layer thickness and a corresponding increase in τ_{wi}. Meanwhile, the temperature profiles show that the flow experiences a slight temperature increase, resulting in an increase in the thermal boundary-layer thickness and thus a decrease in Nu_i.

Between $\hat{\tau}/\hat{\tau}_p$ = 0.31 and 0.50, the temperature profiles demonstrate that the thermal boundary layer continues to grow, thus explaining the continued decay in Nu_i. The velocity profiles show that the velocities away from the wall continue to increase in response to the increase in Re_i. However, as evidenced by the crossing of the $\hat{\tau}/\hat{\tau}_p$ = 0.31 and 0.50 velocity

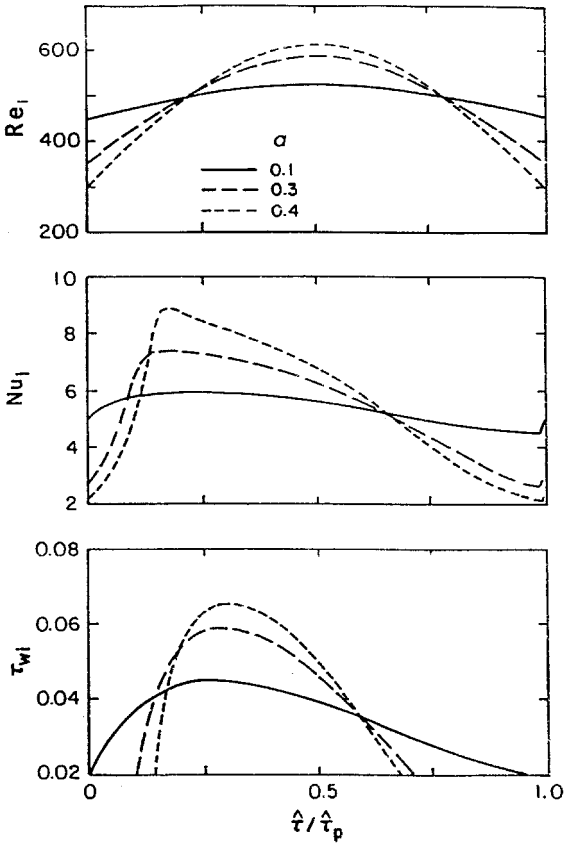

Fig. 5 Effect of amplitude on the cyclic variation of the instantaneous Reynolds number and of the instantaneous Nusselt number and wall shear stress at 5 Hz, Gr/Re = 30.

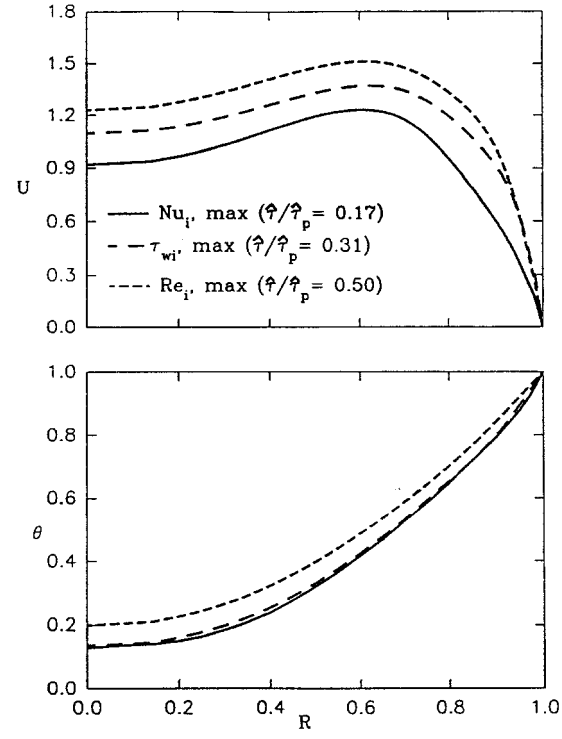

Fig. 6 Velocity and temperature profiles at the maximum Nusselt number, wall shear stress, and Reynolds number instants (Gr/Re = 30, a = 0.4).

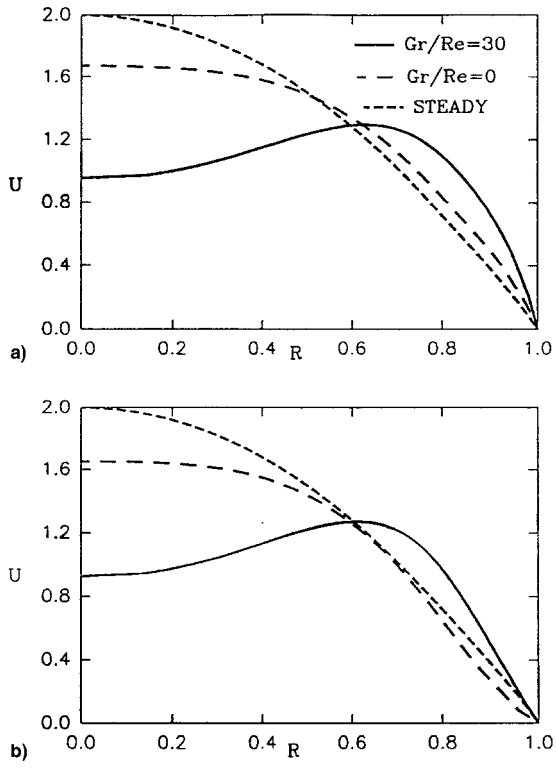

Fig. 7 Comparison of the velocity profiles for the pulsed flow cases (a = 0.1, f = 5 Hz, Gr/Re = 0 and 30) to that for steady, fully developed laminar flow: a) maximum and b) minimum Nusselt number instant.

profiles closer to the wall, the momentum boundary layer actually grows thicker, causing a decrease in τ_{wi}.

Velocity profiles for unpulsed flow (steady, fully developed laminar flow) and for pulsed flow at Gr/Re = 0 and 30 for a = 0.1 and f = 5 Hz at their maximum and minimum Nusselt number instants are compared in Fig. 7. An overview of the figure reveals a hump in the Gr/Re = 30 profile at both the minimum and maximum Nusselt number instants. This hump is caused by the buoyancy effect and is responsible for the large near-wall velocity gradients in the figure. These large gradients are responsible for the fact that Nu_i in Fig. 5 exceeds the steady, fully developed, laminar flow Nusselt number of 3.657.

For Gr/Re = 0, the near-wall velocity gradient for the maximum Nusselt number exceeds that for steady, fully developed laminar flow; whereas the velocity gradient for the minimum Nusselt number lies below that for steady, fully developed laminar flow. The instantaneous Nusselt results for Gr/Re = 0 (not presented) demonstrated that the maximum Nusselt number exceeded the fully developed value; whereas the minimum Nusselt number was less than the fully developed value.

The velocity profiles displayed in Fig. 7 show why the pulsations for Gr/Re = 30 resulted in a decrease in Nu_{av}/τ_{av} compared to the steady, fully developed laminar situation, while the excitations for Gr/Re = 0 resulted in increases as large as 39% in Nu_{av}/τ_{av}.

Frequency Effect

Figure 8 displays the effect of the excitation frequency on the cyclic-averaged Nusselt number and dimensionless wall shear stress at a = 0.1 for both Gr/Re = 0 and 30. The figure shows that for both Gr/Re values the Nusselt number and dimensionless wall shear stress increase with frequency. Regarding Nu_{av}/τ_{av}, at 40 Hz, Nu_{av}/τ_{av} increases by 23% for Gr/Re = 0 and decreases by 5% for Gr/Re = 30, compared to that for steady, fully developed laminar flow (f = 0); whereas at 60 Hz and Gr/Re = 30, Nu_{av}/τ_{av} increases by 5%. The poor performance at Gr/Re = 30 was related to the fact that the buoyancy effect maintains large near-wall velocity gradients.

Figure 9 displays the effect of frequency on the cyclic variation of the instantaneous Nusselt numbers and dimensionless wall shear stresses at a = 0.1 for Gr/Re = 30. As observed in Fig. 5, for the amplitude effect, the Nu_i and τ_{wi} distributions are distorted from the sinusoidal Re_i distribution, with Nu_i and τ_{wi} reaching their peak values before Re_i. However, both the peak Nu_i and τ_{wi} locations migrate toward the peak Re_i location with increasing frequency. The figure also shows that the peak Nu_i value occurs before the peak τ_{wi} value.

Velocity profiles for 5 and 40 Hz at their respective maximum Nusselt number instants are displayed in Fig. 10 for a =

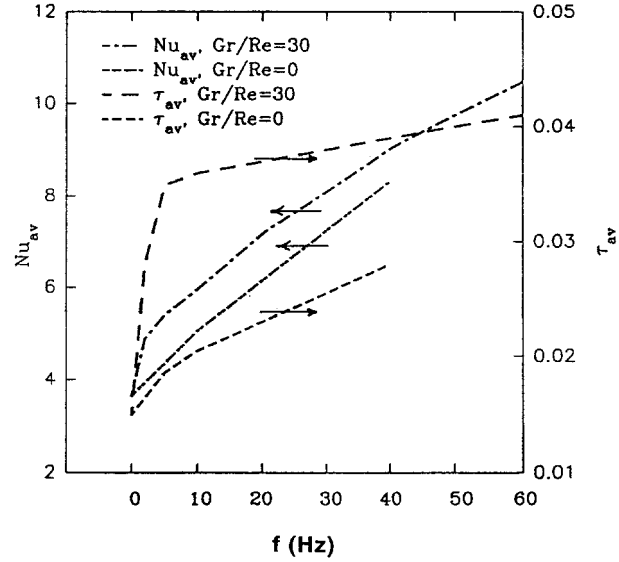

Fig. 8 Effect of frequency on the cyclic-averaged Nusselt number and dimensionless wall shear stress, a = 0.1.

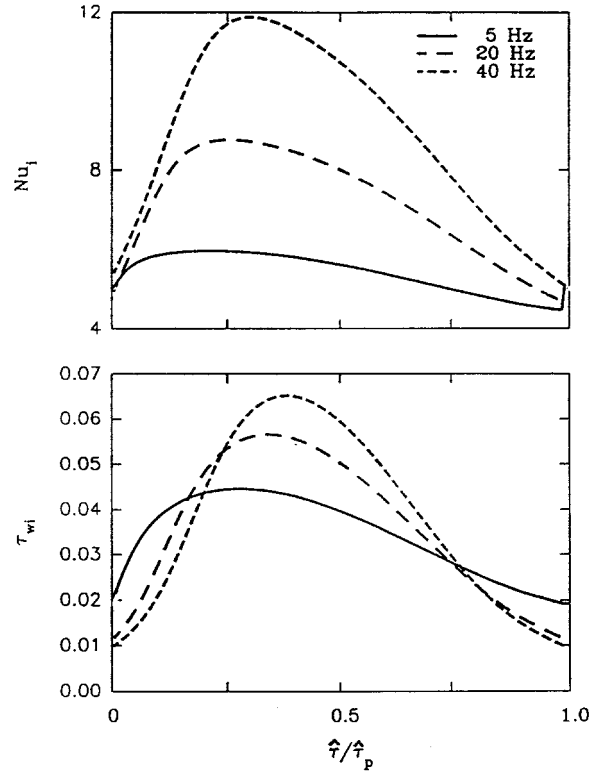

Fig. 9 Effect of frequency on the cyclic variation of the Nusselt number and dimensionless wall shear stress at a = 0.1, Gr/Re = 30.

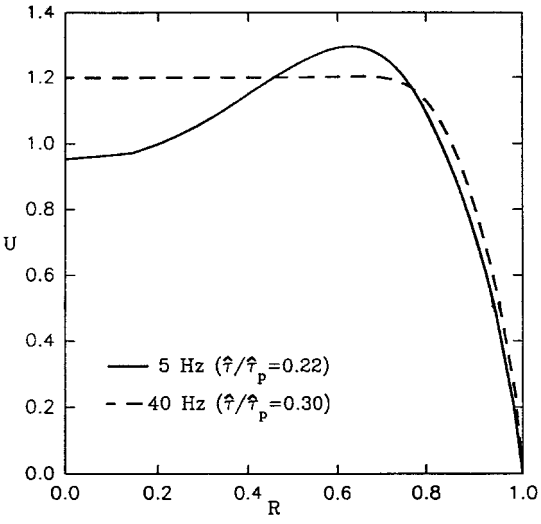

Fig. 10 Velocity profiles at the maximum Nusselt number instant for different frequencies, a = 0.1, Gr/Re = 30.

0.1. The buoyancy-induced hump is clearly present at 5 Hz. On the other hand, the absence of the hump at 40 Hz suggests that the role of the buoyancy force at 40 Hz is less than at 5 Hz and that the development of the flow is strongly influenced by the flow pulsation. At 5 Hz, the near-wall acceleration of the fluid caused by buoyancy strongly manifests itself and leads to the central concavity in the velocity profile. At 40 Hz the near-wall acceleration is adversely affected and the profile is flatter.

Conclusions

It is concluded from the preceding presentation of numerical results that superposing sinusoidal-like velocity pulsations on a laminar steady flow (with and without buoyancy) in an isothermal-walled vertical tube results in cyclic-averaged Nusselt numbers Nu_{av} that are greater than the steady, fully developed laminar-flow value. As expected, Nu_{av} was larger in the presence of buoyancy (Gr/Re = 30) for a common frequency and amplitude than in the absence of buoyancy (Gr/Re = 0). At a low amplitude (a = 0.1), Nu_{av} increased with increasing frequency for both Gr/Re = 0 and 30. At the lowest frequency considered (5 Hz), Nu_{av} increased with amplitude for Gr/Re = 0, but after a rather large increase in Nu_{av} between a = 0 and 0.1, Nu_{av} was rather insensitive to further increases in the amplitude for Gr/Re = 30 over the amplitude range studied.

Although the effect of buoyancy resulted in higher Nu_{av} values, they were more than compensated for by accompanying increases in τ_{av}. From the standpoint of enhancement, where frictional effects are included, pulsing a flow with buoyancy typically leads to either negligible increases or even decreases in Nu_{av}/τ_{av} compared to that for steady, fully developed laminar flow, with the maximum degradation being 34% for a = 0.1 and f = 5 Hz. Conversely, pulsing a flow without buoyancy resulted in increases as high as 39% over the steady, fully developed laminar value for a = 0.8 and f = 5 Hz.

References

[1]Martinelli, R. C., Boelter, L. M. K., Weinberg, E. B., and Yakahi, S., "Heat Transfer to a Fluid Flowing Periodically at Low Frequencies in a Vertical Tube," *Transactions of the American Society of Mechanical Engineers*, Vol. 65, June 1943, pp. 789–798.

[2]Jackson, T. W., Harrison, W. B., and Boteler, W. C., "Free Convection, Forced Convection, and Acoustic Vibrations in a Constant Temperature Vertical Tube," *Journal of Heat Transfer*, Vol. 81, Feb. 1959, pp. 68–74.

[3]Lemlich, R., and Hwu, C., "The Effect of Acoustic Vibration on Forced Convective Heat Transfer," *AIChE Journal*, Vol. 7, March 1961, pp. 102–106.

[4]Purdy, K. R., Jackson, T. W., and Gorton, C. W., "Viscous Fluid Flow Under the Influence of a Resonant Acoustic Field," *Journal of Heat Transfer*, Vol. 86, May 1964, pp. 97–106.

[5]Jackson, T. W., and Purdy, K. R., "Resonant Pulsating Flow and Convective Heat Transfer," *Journal of Heat Transfer*, Vol. 87, Sept. 1965, pp. 507–512.

[6]Grassmann, P. P., and Tuma, M., "Applications of the Electrolytic Method—II. Mass Transfer Within a Tube for Steady, Oscillating and Pulsating Flows," *International Journal of Heat and Mass Transfer*, Vol. 22, June 1979, pp. 799–804.

[7]Kirmse, R. E., "Investigations of Pulsating Turbulent Pipe Flow," *Journal of Fluids Engineering*, Vol. 101, Dec. 1979, pp. 436–442.

[8]Ramaprian, B. R., and Tu, S., "An Experimental Study of Oscillatory Pipe Flow at Transitional Reynolds Numbers," *Journal of Fluid Mechanics*, Vol. 100, Oct. 1980, pp. 513–544.

[9]Creff, R., Batina, J., Andre, P., and Karunanithi, V. S., "Numerical Model for Dynamic and Thermal Developments of a Pulsed Laminar Ducted Flow," *Numerical Heat Transfer*, Vol. 6, Sept. 1983, pp. 173–188.

[10]Liao, N. S., Wang, C. C., and Hong, J. T., "An Investigation of Heat Transfer in Pulsating Turbulent Pipe Flow," *Fundamentals of Forced and Mixed Convection, Proceedings of the ASME 23rd National Heat Transfer Conference*, HTD, Vol. 92, American Society of Mechanical Engineers, New York, 1985, pp. 53–60.

[11]Siegal, R., "Influence of Oscillation-Induced Diffusion on Heat Transfer in a Uniformly Heated Channel," *Journal of Heat Transfer*, Vol. 109, Feb. 1987, pp. 244–247.

[12]Dec, J. E., and Keller, J. O., "Pulse Combustor Tail-Pipe Heat-Transfer Dependence on Frequency, Amplitude, and Mean Flow Rate," *Combustion and Fluids*, Vol. 77, Sept. 1989, pp. 359–374.

[13]Zeldin, B., and Schmidt, F. W., "Developing Flow with Combined Free and Forced Convection in an Isothermal Vertical Tube," *Journal of Heat Transfer*, Vol. 94, May 1972, pp. 211–223.

[14]Patankar, S. V., and Spalding, D. B., *Heat and Mass Transfer in Boundary Layers*, 2nd ed., Intertext, London, 1970.